ACS OMEGA

http://pubs.acs.org/journal/acsodf

Article

Systematic Design and Study of Star-like Polymeric Prodrug Unimolecular Micelles β-CD-P[CL-*co*-(ACL-*g*-DOX)-SS-MPEG]$_{21}$ by DPD Simulations

Zexiong Yang, Haiyan Mai, Delin Wang, Teng He, Fang Chen, and Chufen Yang*

Cite This: *ACS Omega* 2023, 8, 4963−4971

Read Online

ACCESS | Metrics & More | Article Recommendations

ABSTRACT: Unimolecular micelles composed of a single polymeric molecule have recently attracted significant attention in anti-cancer drug delivery due to their high thermodynamic stability and small particle sizes. Applying the prodrug strategy to unimolecular micelles may provide superior nano-drug carriers with simultaneous high stability, low drug leakage, and well-drug loading capacity. However, the formation mechanism of the unimolecular prodrug micelles, the superiority of the prodrug strategy, as well as the prodrug controlled release mechanism were scantily understood at the mesoscopic scale. In this work, dissipative particle dynamics mesoscopic simulations were employed to investigate the self-assembly behavior, formation conditions, drug distribution regularities, and the prodrug release process of the star-like polymeric prodrug unimolecular micelles formed by β-CD-P[CL-*co*-(ACL-*g*-DOX)-SS-MPEG]$_{21}$. A special bond-breaking script was used to accomplish the bond-breaking simulation of the grafted DOX bonds and the disulfide bonds. Results showed that to form well monodispersed and superior DOX-loaded unimolecular micelles, the polymer concentration should be well controlled at low volume fractions (≤10.59%), and the detailed molecular structure of the polymer was suggested as β-cyclodextrin-P[caprolactone-*co*-(amino caprolactone-*g*-doxorubicin)-disulfide-methyl polyethylene glycol]$_{21}$) (β-CD-P[CL_{30}-*co*-$(ACL\text{-}g\text{-}DOX)_8$-SS-$MPEG_{49}$]$_{21}$). By comparison with the DOX physically loaded micelles, it was found that the prodrug unimolecular micelles with DOX grafted on the polymer displayed no drug leakage and superior drug loading capacity. Simulations on the prodrug release process showed that the prodrug unimolecular micelles assembled by β-CD-P[CL_{30}-*co*-$(ACL\text{-}g\text{-}DOX)_8$-SS-$MPEG_{49}$]$_{21}$ would provide good dual pH/reduction-responsive DOX release performance.

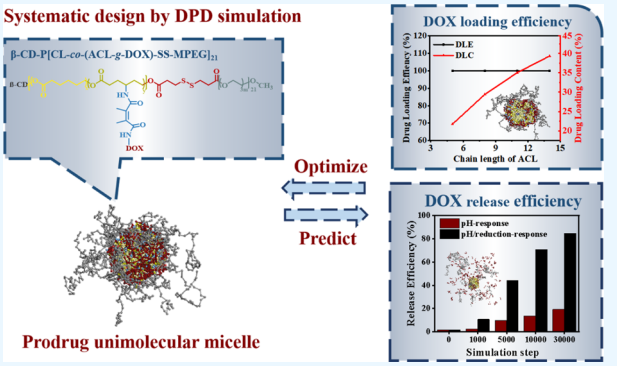

1. INTRODUCTION

Nano-drug delivery system has been demonstrated to be a useful strategy for improving the therapeutic effect of anticancer drugs and reducing their side effects due to the existence of enhanced permeability and retention effect in tumor tissues.[1,2] Among them, nano-polymeric micelles assembled from amphiphilic polymers have shown unique advantages in enhancing the solubility of hydrophobic anticancer drugs and being easy to functionalize.[3−5]

Although great achievements have been made in nano-polymeric micelles, the stability of the polymeric micelles is still needed to improve. Since both the formation and the stabilization of conventional micelles require the polymer concentration to be above the CMC value, when annotated in vivo, the polymeric micelles will become thermodynamically unstable under the influence of hemodilution and may dissociate into individual molecules.[6,7] Unimolecular micelles can help to overcome this issue. As its name suggests, a unimolecular micelle is composed of a single polymeric molecular, which can be formed at low concentrations even below the CMC, thus exhibiting better stability and not easily influenced by environmental conditions or hemodilution, which means showing an advantage of long periods of circulation.[8,9] Generally, the preparation of unimolecular micelles is based on dendrimers,[10] hyperbranched polymers,[11] and star polymers.[12,13] Among them, star polymers are easier to synthesize, and by regulating the ratio of their hydrophilic and hydrophobic segments, one can easily obtain unimolecular micelles with good performance of drug delivery.[14]

Despite many studies having demonstrated that the drug delivery effect of nano-micelles has more advantages than that

Received: November 17, 2022
Accepted: January 16, 2023
Published: January 26, 2023

https://doi.org/10.1021/acsomega.2c07371
ACS Omega 2023, 8, 4963−4971

of conventional drugs, most polymeric micelles, including unimolecular micelles, still have the problems of drug leakage in advance during the drug delivery.[15,16] These problems boost toxic side effects at non-disease sites, lower the expected therapeutic effect, and even cause multiple drug resistance.[17] The prodrug's polymeric micelles that connect the drug with dynamic covalent bonds into the polymeric molecules can efficiently overcome the problem of drug leakage in advance.[18−20] Moreover, compared with the physically drug-loaded micelles, the drug-loading capacity of the prodrug micelles is determined by the functional groups of the polymer, which can be effectively improved by increasing the amount of the corresponding functional groups.[21,22] Therefore, applying the prodrug strategy to unimolecular micelles may simultaneously overcome the problems of easy dissociation, drug leakage in advance, and the low drug-loading capacity of the traditional polymeric micelles.

In this work, wewould like to design a dual pH/reduction-responsive star-like polymeric prodrug unimolecular micelles β-cyclodextrin-P[caprolactone-*co*-(amino caprolactone-*g*-doxorubicin)-disulfide-methyl polyethylene glycol]$_{21}$) (β-CD-P[CL-*co*-(ACL-*g*-DOX)-SS-MPEG]$_{21}$) for DOX delivery. In this prodrug unimolecular micelles, β-CD is used as the center of the polymer, providing 21 −OHs to synthesize a 21-arm star-like block polymer.[23] Amino caprolactones are inserted into the hydrophobic PCL chain to provide binding sites for doxorubicin grafted by 2,3-dimethyl maleic anhydride to form pH-responsive β-carboxylic amide bonds, which would be cleaved at the slightly acidic condition of tumor microenvironment and release DOX.[24] A disulfide linkage (−SS−) is used to connect the hydrophilic MPEG block and the hydrophobic chain, which has been demonstrated to be effective in conferring the polymer reduction-responsive characteristics.[25]

Using computer simulation methods to investigate the self-assembly behaviors and drug loading/release behaviors of the polymeric micelles at the mesoscopic level and subsequently seek improving directions based on the simulation results is a potential way to save the exploitation period. For example, Guo et al. used the dissipative particle dynamics (DPD) method to simulate the self-assembly and stimuli-response behavior of the micelles formed by amphiphilic polymers and deemed the DPD simulation a useful tool to provide qualitative information for drug delivery systems.[26] Wu et al. investigated the structure−property relationship of star-like polymer micelles with DPD simulation and provided theoretical guidance for the structure design and proportional optimization of polymer micelles.[27] Zhou et al. simulated the drug loading/release behaviors of unimolecular micelles and further explained the difference between zwitterionic DDS and PEGylated DDS at the mesoscopic level.[28] Zhang et al. reported the systematic design and application of unimolecular star-like block copolymer micelles and revealed the formation process of unimolecular micelles using DPD simulations.[29] In our previous work, by establishing a special disulfide bond-breaking script, the self-assembly behavior of reduction-responsive polymeric micelles and their drug release process were studied, providing a practical mesoscopic simulation approach for the polymeric micelles that involved the cleavage of chemical bonds.[30,31]

Although abundant experimental studies of prodrug micelles have been reported, their self-assembly and drug delivery, especially drug release behavior, have been poorly investigated at the mesoscopic scale.[32] In this work, DPD simulations were employed to investigate the self-assembly behavior and drug controlled release process of the star-like prodrug polymeric unimolecular micelles β-CD-P[CL-*co*-ACL(-DOX)]-SS-MPEG. During this process, the formation mechanism of the unimolecular prodrug micelles and the superiority mechanism of the prodrug strategy that was scantily understood at the mesoscopic scale were explored. The mechanism of how the combination of pH-responsive β-carboxylic amide bonds and reduction-responsive disulfide bonds improved the DOX controlled release property was also discussed. This study can provide valuable information for the experimental optimization and property prediction of the dual pH/reduction-responsive unimolecular prodrug micelles.

2. DPD SIMULATION

2.1. DPD Method. DPD simulation is a mesoscopic simulation method that is suitable to study polydisperse multiphase systems, such as the self-assembly behavior and drug release process of polymeric micelles.[33,34] In this method, the molecular will be divided into several fragments known as coarse-graining beads to avoid the large amount of computational work and conserve the key characteristics and behaviors of systems. In the DPD simulation, the force ($\mathbf{f}_{ij}$) between each pair of beads is the sum of a conservative force ($\mathbf{F}_{ij}^{C}$), a dissipative force ($\mathbf{F}_{ij}^{D}$), and a random force ($\mathbf{F}_{ij}^{R}$), which are given by the following equations[35,36]

$$\mathbf{F}_{ij}^{C} = \begin{cases} a_{ij}(1 - r_{ij})\hat{\mathbf{r}}_{ij} & (r_{ij} < 1) \\ 0 & (r_{ij} \geq 1) \end{cases} \tag{1}$$

$$\mathbf{F}_{ij}^{D} = -\frac{\sigma^2(\omega(r_{ij}))^2}{2kT}(\hat{\mathbf{r}}_{ij}\cdot\mathbf{v}_{ij})\hat{\mathbf{r}}_{ij} \tag{2}$$

$$\mathbf{F}_{ij}^{R} = \frac{\sigma\omega(r_{ij})\hat{\mathbf{r}}_{ij}\zeta}{\sqrt{\delta_t}} \tag{3}$$

where a_{ij} is the interaction parameter between beads i and j, $r_{ij} = |\mathbf{r}_{ij}|$, $\hat{\mathbf{r}}_{ij} = \mathbf{r}_{ij}/|\mathbf{r}_{ij}|$, $\hat{\mathbf{r}}_{ij} = \mathbf{r}_{ij}/|\mathbf{r}_{ij}|$, σ denotes the noise strength, $v_{ij} = v_i - v_j$, k is the Boltzmann constant, T denotes the system temperature, ζ is a randomly fluctuating variable with zero mean and unit variance, δ_t is the time step of simulation, $\omega(r) = (1-r)$ for $r < 1$ and $\omega(r) = 0$ for $r > 1$ are the r-dependent weight functions. The interaction parameter a_{ij} can be calculated by eq 4[30,37]

$$a_{ij} = a_{ii} + 3.27\chi_{ij} \tag{4}$$

where a_{ii} is equal to 25 according to the work of Groot and Warren[35,36] when the particle density is set as 3, χ_{ij} is the Flory−Huggins parameter. For polar components or components with hydrogen bonding, χ_{ij} can be calculated by eq 5[38]

$$\chi_{ij} = \frac{\Delta E_{mix} V_r}{RT\phi_i\phi_j V} \tag{5}$$

where ΔE_{mix} is the mixing energy of the binary components obtained by the potential energy of the binary mixture, V is the total volume, V_r is the reference volume, R is the gas constant, and T is temperature; ϕ_i and ϕ_j are the volume fractions of beads i and j, respectively.[38]

In the case of nonpolar components without hydrogen bonding, χ_{ij} is estimated by the following equation[39,40]

https://doi.org/10.1021/acsomega.2c07371
ACS Omega 2023, 8, 4963−4971

$$\chi_{ij} = \frac{(\delta_i - \delta_i)^2 V_{bead}}{RT} \quad (6)$$

where δ_i and δ_j are the solubility parameters of beads i and j, V_{bead} is the average of molar volumes of all the beads, which are obtained by molecular dynamics simulations.

The spring force $\mathbf{F}_{ij}^{S} = C\mathbf{r}_{ij}$ describes the constraint between the beads, which are connected in molecules. In this work, the spring constant C was set as 4, a slightly smaller distance for bonded beads compared to non-bonded ones, which is enough to keep the adjacent beads connected along the polymer backbone.

2.2. Coarse-Grained Models and Interaction Parameters. The self-assembly and drug delivery behavior of the star-like polymeric prodrug unimolecular micelles β-CD-P[CL-*co*-(ACL-*g*-DOX)-SS-MPEG]$_{21}$ were investigated by DPD simulations, whose coarse-grained models are shown in Figure 1. The polymer β-CD-P[CL-*co*-(ACL-*g*-DOX)-SS-MPEG]$_{21}$

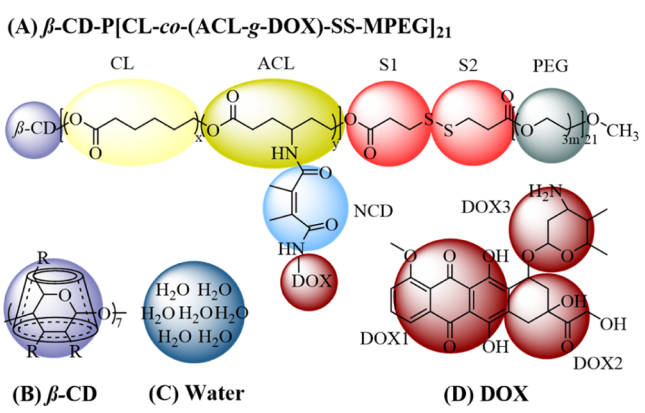

Figure 1. Coarse-grained models of (A) β-CD-P[CL-*co*-(ACL-*g*-DOX)-SS-MPEG]$_{21}$, (B) β-CD, (C) water, and (D) DOX.

was divided into β-CD (violet), PCL (spry), ACL (mustard), S1 (red), S2 (red), NCD (blue), and PEG (gray); DOX (crimson) was divided into DOX1, DOX2, and DOX3; to make the mass of all beads as close as possible, seven water molecules were represented as a single water bead (steel blue).

The interaction parameters (a_{ij}) between different beads were calculated according to our previous method[30,41] and listed in Table 1. In this work, 130.8 amu average mass, 204.3 Å^3 average volume, and 3.7 Å average radius of each bead were used. With the bead density set as 3, the cut-off radius R_c in the DPD simulations was 8.495 Å. A 30 × 30 × 30 R_c^3 box with periodic boundary conditions was applied in each simulation. The integration time step was set at 0.05 τ, where τ defined as $\tau = (mr_C^2/k_BT)^{1/2}$ is the reduced DPD time unit,[35,36] and the simulation step was 100,000 steps, which was found to achieve the simulation equilibrium state.

2.3. Disulfide and β-Carboxylic Amide Bond-Breaking for DOX Release Simulation. The disulfide (−S1−S2−) and β-carboxylic amide (NCD-DOX) bond-breaking simulations were carried out using a special bond-breaking script developed on the nearest media-bead bond-breaking principle according to the following four-step cyclic dynamic processes:[30,31]

a. DPD coarse-grain models comprised of the pre-cleavage disulfide (−S1−S2−) bead pairs or β-carboxylic amide (NCD-DOX) bead pairs were constructed, and imported the original bead forcefield.
b. Set probabilities of bond-breaking for S1 and S2 bead pairs or NCD and DOX bead pairs, and the bonds randomly broken based on probability.
c. Reassigned bead types for S1 and S2 bead pairs to be S1H and S2H, or for NCD and DOX bead pairs to be NCDH and DOXH, then ran a short step DPD simulation to relax the cell.
d. Once the pre-assigned probability of bond breaking was reached, the bond breaking process was terminated, or the probability of bond breaking was reset and steps b−c repeated.

With the cleavage of the disulfide bond, the hydrophilic SH-PEG block departed away from the whole polymer, and correspondingly, the S1 and S2 beads would transform into S1H and S2H beads, while the cleavage of β-carboxylic amide bond resulted in DOXH departed away, with the corresponding ACL, NCD, and DOX3 beads transformed into ACLH, NCDH, and DOX3H beads. Based on the output results of the bond-breaking simulation, new interaction parameters would be reassigned for the transformed beads to simulate the

Table 1. Interaction Parameters (a_{ij}) between Different Beads Used in DPD Simulation

a_{ij}	β-CD	CL	ACL	ACLH	NCD	NCDH	S1	S1H	S2	S2H	PEG	DOX1	DOX2	DOX3	DOX3H	water
β-CD	25.0															
CL	50.0	25.0														
ACL	50.0	27.3	25.0													
ACLH	100.0	61.5	25.0	25.0												
NCD	50.0	25.1	39.7		25.0											
NCDH	100.0	55.1		21.6		25.0										
S1	50.0	25.8	25.6		26.0		25.0									
S1H	100.0	25.8		42.5		48.8		25.0								
S2	50.0	25.8	25.6		26.0		25		25.0							
S2H	100.0	25.8		42.5		48.8		25.0		25.0						
PEG	50.0	32.5	27.5	27.1	26.7	24.1	30.0	22.3	30.0	22.3	25.0					
DOX1	50.0	27.5	26.3	51.5	25.3	41.3	25.1	35.4	25.1	35.4	30.7	25.0				
DOX2	50.0	30.4	25.3	26.8	25.8	28.8	25.6	26.4	25.6	26.4	26.8	26.3	25.0			
DOX3	50.0	35.1	25.1		25.1		25.3		25.3		28.4	26.1	25.4	25.0		
DOX3H	100.0	97.3		24.2		25.1	25.6	20.3	25.6	20.3	20.8	26.1	25.4		25.0	
WATER	50.0	77.8	27.5	12.6	42.3	10.3	74.5	10.2	74.5	10.2	26.1	45.2	27.9	23.6	8.6	25.0

https://doi.org/10.1021/acsomega.2c07371
ACS Omega 2023, 8, 4963−4971

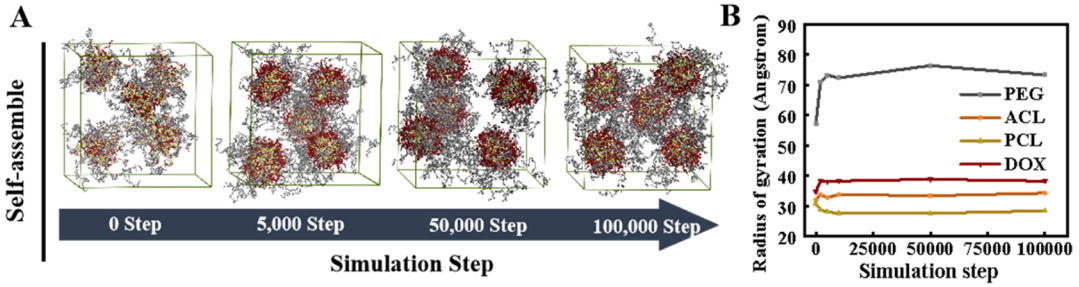

Figure 2. Morphologies of the prodrug unimolecular micelles at different simulation steps (A) and the corresponding ROG curves (B).

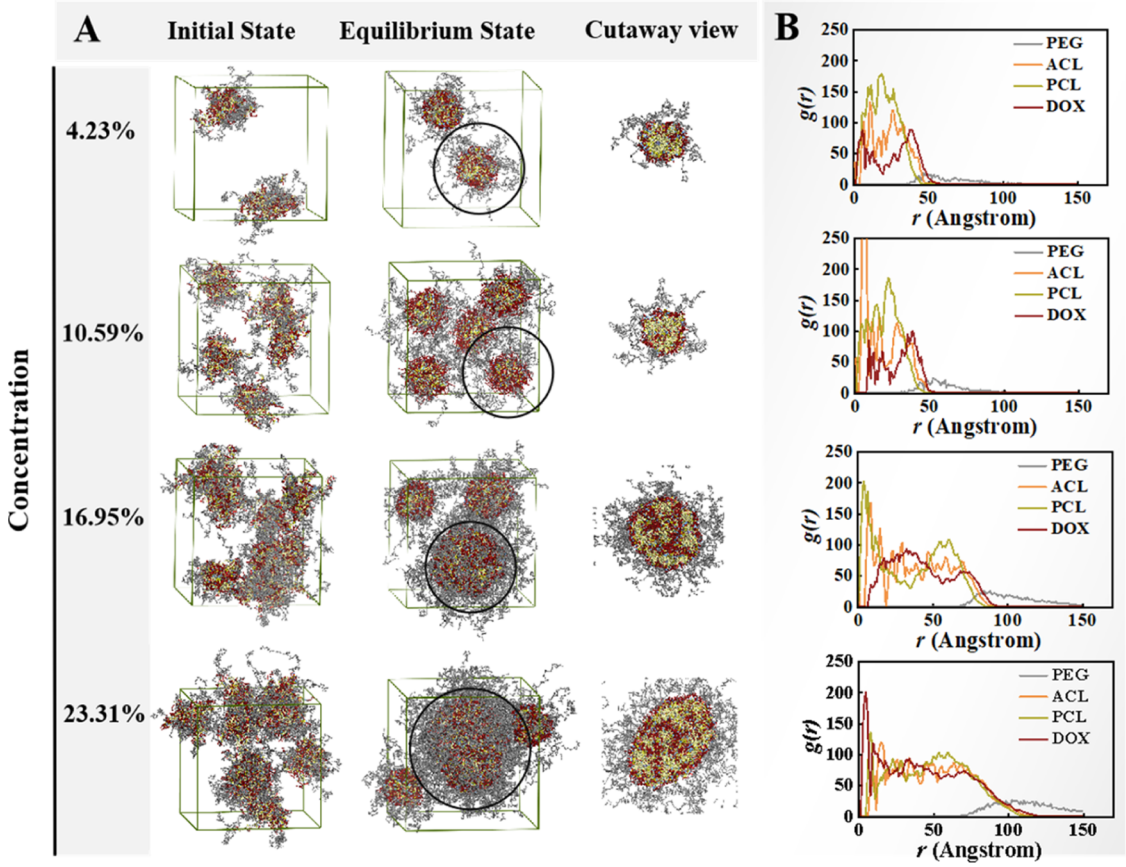

Figure 3. Aggregation morphologies (A) at different polymer concentrations and their RDF curves (B) at the equilibrium state.

reduction-responsive detachment of the protective PEG layer and the pH-responsive DOX release process. In addition, the pH value of this work was set as 5.0 to simulate the slightly acidic condition of the tumor microenvironment, in which the pH-sensitive β-carboxylic amide (NCD-DOX) bonds would completely break.

3. RESULTS AND DISCUSSION

3.1. Self-Assembled Behavior of the Polymeric Prodrug Unimolecular Micelles. In DPD simulation, the self-behavior process could be observed through directly mixing the polymer molecules with water beads in the box and setting forcefield parameters to drive the system to achieve a new dynamic equilibrium. The self-assembled evolution process of the prodrug unimolecular micelles β-CD-P[CL_{30}-*co*-(ACL-*g*-DOX)$_8$-SS-$MPEG_{49}$]$_{21}$ was captured by a series of snapshots as shown in Figure 2A, with 10.59% volume fraction of polymer and 89.41% volume fraction of water.

It was found that a star-like β-CD-P[CL-*co*-(ACL-*g*-DOX)-SS-MPEG]$_{21}$ molecule was expected to self-assemble into one unimolecular micelle in an aqueous solution. At the beginning (0 step), 10.59% volume fraction of β-CD-P[CL_{30}-*co*-(ACL-*g*-DOX)$_8$-SS-$MPEG_{49}$]$_{21}$ which could exactly formed into five star-like unimolecular micelles were randomly dispersed into 89.41% volume fraction of water. As the simulation went on, caused by the spontaneous separation phenomenon of the hydrophobic and hydrophilic blocks, the hydrophobic beads of CL, ACL, and DOX aggregated to form the core of the unimolecular micelles, while the hydrophilic beads of PEG spread to the outside and formed the hydrophilic shell of the unimolecular micelles (5000 steps). As the simulation step was increased to 10, 000, or even continuing to increase the simulation step to 100, 000, no obvious change was found on the morphologies and sizes of the unimolecular micelles, indicating that the microphase separation of this unimolecular micellar system had reached dynamic equilibrium. The

https://doi.org/10.1021/acsomega.2c07371
ACS Omega 2023, 8, 4963−4971

dynamic equilibrium could be further confirmed by the radius of gyration (ROG) curves of PEG, PCL, ACL, and DOX beads, as shown in Figure 2 (B). All the ROG curves remained mostly unchanged after 10, 000 steps, mainly consistent with the visual inspection of Figure 2 (A). It meant that the star-like polymer β-CD-P[CL-*co*-(ACL-*g*-DOX)-SS-MPEG]$_{21}$ could self-assemble into unimolecular micelles with a significantly shorter time compared to those non-unimolecular micelles formed by linear polymers in the previous studies,[30,31] which was possible because the self-assemble of unimolecular micelles took place inside the polymer molecules, and the intramolecular distribution of the hydrophilic and hydrophobic segment was in accordance with the core−shell structure. This indicated that the self-assembly time could be appropriately shortened when preparing the prodrug's unimolecular micelles.

3.2. Effect of Polymer Concentration on Micellar Aggregation Morphology. By increasing the polymer concentration in the simulation system, the unimolecular micelles might form into multimolecular micelles or micellar aggregates, as shown in Figure 3. When the initial number of star-like β-CD-P[CL_{30}-*co*-$(ACL\text{-}g\text{-}DOX)_8$-SS-$MPEG_{49}]_{21}$ was increased to 8 (16.95% volume fraction) and 11 (23.31% volume fraction), the transition between unimolecular micelles and aggregations was observed. Compared to the simulation system with a 10.59% volume fraction of polymer, at equilibrium state, large multimolecular aggregates and small unimolecular micelles were both found in the two higher concentration systems. While decreasing the initial number of the polymer molecules to 2 (4.23% volume fraction), the system kept well monodispersity the same as the system with 10.59% volume fraction of polymer. Cutaway views of the four concentration micelles revealed the large multimolecular aggregates showed a similar core−shell structure compared to the small unimolecular micelles, despite the hydrophobic cores of the multimolecular aggregates assembled by PCL and ACL beads, together with most of the DOX beads, while in the unimolecular micelles, most of the DOX beads were distributed at the interface between the hydrophobic cores and the hydrophilic shell. This could be further confirmed by the radial distribution function (RDF) curves, which can quantitatively describe the interior structure of the micelles. In the RDF curves, the value of $g(r)$ represented the chosen bead distribution probability at the radial distance, with the coordinate of the reference molecule as the micellar center. As shown in Figure 3B, the three micelles had similar core−shell structures that all the MPEG beads spread outside the core to form the hydrophilic shell, and DOX, PCL, and ACL beads assembled to form the hydrophobic core, though in the unimolecular micelles, the peak of the RDF curve for DOX beads appeared at the interface, which was consistent with the cutaway views.

Therefore, to improve the monodispersity of unimolecular micelles, the polymer concentration should be well controlled in low volume fraction ($\leq$10.59%) in this star-like β-CD-P[CL-*co*-(ACL-*g*-DOX)-SS-$MPEG]_{21}$ system.

3.3. Effect of PCL Chain Length on Micellar Aggregation Morphology. In the star-like β-CD-P[CL-*co*-(ACL-*g*-DOX)-SS-$MPEG]_{21}$ molecule, the chain length of the hydrophobic PCL block played an important role in the drug loading capacity for its assembled unimolecular micelle. In addition to form the micellar core, the hydrophobic PCL block also afforded to reduce the steric hindrance of the grafted DOX. Therefore, to improve the DOX loading capacity, the chain length of the hydrophobic PCL block should be as long as possible, while to avoid the aggregation of the unimolecular micelles, the PCL chain length would be limited.

Here, DPD simulations on the prodrug unimolecular micelles β-CD-P[CL_x-*co*-$(ACL\text{-}g\text{-}DOX)_8$-SS-$MPEG_{49}]_{21}$ with four progressive PCL chain lengths (x = 20, 30, 40, and 50) were performed, and the results are shown in Figure 4. It was found that when the PCL chain length was 20 or 30, the equilibrium aggregation morphology of the prodrug unimolecular micelles displayed well monodispersity, with five unimolecular micelles existing, while when the PCL chain length reached more than 40, the small unimolecular micelles gradually formed into large multimolecular micellar aggregations, with only four or three aggregations existing.

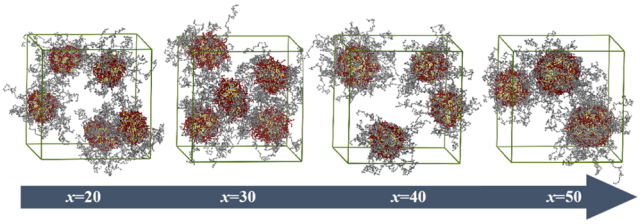

Figure 4. Equilibrium aggregation morphologies of the prodrug unimolecular micelles with different PCL chain lengths.

Accordingly, to keep high monodispersity of the prodrug unimolecular micelles, the PCL chain length was suggested to be set below 40, while to achieve good DOX loading capacity, the PCL chain length should be as long as possible. Therefore, the PCL chain length in this system was suggested to be set as 30.

3.4. Effect of PEG Chain Length on Aggregation Morphology. To decide the appropriate hydrophilic PEG chain length, the contradiction between micellar stability and DOX loading capacity should be fully considered. In the unimolecular micellar system, the longer hydrophilic PEG chain length could not only maintain the micellar stability better but also play an important role in avoiding the aggregation of the unimolecular micelles. However, the longer hydrophilic PEG chain length often resulted in the lower DOX loading capacity of the micelles.

In the DPD simulations of the prodrug unimolecular micelles β-CD-P[CL_{30}-*co*-$(ACL\text{-}g\text{-}DOX)_8$-SS-$MPEG_m]_{21}$ system, four different PEG chain lengths (m = 27, 38, 49, and 60) were set, and their corresponding equilibrium aggregation morphologies of simulation results are shown in Figure 5. It showed that when the hydrophilic PEG chain length was 27 or 38, there were only four or three micellar aggregations existing in the simulation box, indicating that some of the unimolecular micelles were gathering into large multimolecular aggregates,

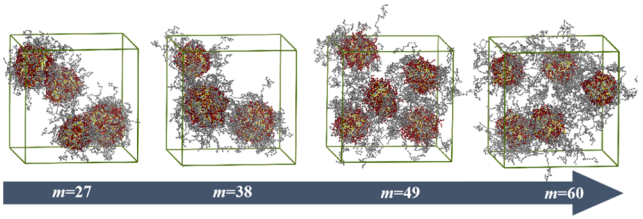

Figure 5. Equilibrium aggregation morphologies of the prodrug unimolecular micelles with different PEG chain lengths.

https://doi.org/10.1021/acsomega.2c07371
ACS Omega 2023, 8, 4963−4971

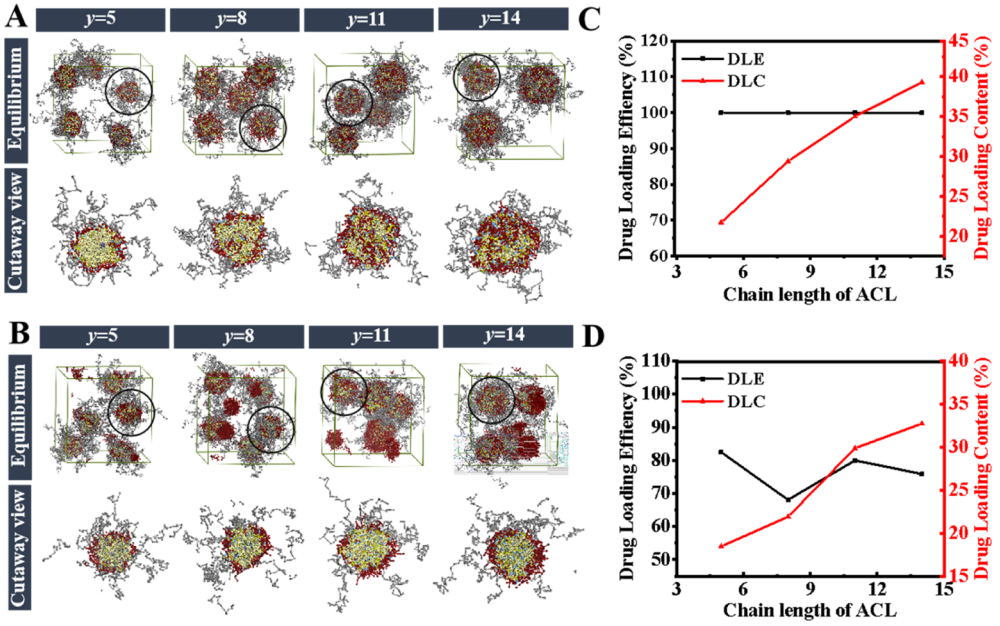

Figure 6. Equilibrium aggregation morphologies and cutaway views of the prodrug micelles (A) and the DOX physically loaded micelles (B) and DLE/DLC curves of the prodrug micelles (C) and the DOX physically loaded micelles (D).

while when the hydrophilic PEG chain length was 49 or 60, the five unimolecular micelles kept well monodispersity in the simulation box, due to their hydrophilic PEG chain length being long enough to shield the aggregation tendency caused by hydrophobic interaction of the micellar core. In order to coordinate the stability of unimolecular micelles and their DOX loading capacity, the hydrophilic PEG chain length was suggested to be set as 49.

3.5. ACL Chain Length and DOX Loading Capacity. In the drug delivery system of polymeric prodrug unimolecular micelles, the drug loading capacity was associated with the ACL chain length since the loaded DOX was directly grafted on the amino group of the ACL segment. To enhance the DOX loading capacity, the amounts of ACL should be as more as possible. However, due to the hydrophobic nature of DOX, simply pursuing high DOX loading would compel the unimolecular micelles to aggregate. Therefore, the amounts of ACL monomer in the polymeric molecule might be limited.

To obtain the appropriate ACL chain length of the polymer, DPD simulations were carried out for the prodrug unimolecular micelles β-CD-P[CL_{30}-*co*-(ACL-*g*-DOX)$_y$-SS-$MPEG_{49}$]$_{21}$ with four different ACL chain lengths (y = 5, 8, 11, and 14), and the results are shown in Figure 6A. It showed that when the ACL chain length was 5 or 8, the polymer micelles could maintain well monodispersity, while when it increased to 11 or 14, one or two multimolecular aggregations appeared. The relationships between drug loading efficiency (DLE)/drug loading content (DLC) and ACL chain length were further investigated to quantitatively analyze the drug loading capacity of prodrug unimolecular micelles, as shown in Figure 6C. The DLE and DLC were calculated by the following equation[42]

$$\mathrm{DLE}_{(\mathrm{vol}\%)} = \frac{\text{DOX beads number loaded in the micelles}}{\text{DOX beads number in the box}} \times 100\% \quad (7)$$

$$\mathrm{DLC}_{(\mathrm{vol}\%)} = \frac{\text{DOX beads number loaded in the micelles}}{\text{All beads number in the micelles}} \times 100\% \quad (8)$$

In Figure 6C, it was found that the DLC value gradually rose as the chain length of ACL, while the DLE values being set as 100% by default due to all DOX beads were grafted on the ACL beads through NCD beads in the prodrug micelles system. From the DLC curves, the chain length of ACL y = 14 would provide a higher DLC value than that of y = 5, 8, or 11. However, to maintain the high monodispersity of the prodrug unimolecular micelles, the ACL chain length was suggested to be set as y = 8.

To verify the superiority of the prodrug strategy, contrast DPD simulations of the DOX physically loaded micelles were carried out with the same import parameters of the β-CD-P[CL_{30}-*co*-(ACL-*g*-DOX)$_y$-SS-$MPEG_{49}$]$_{21}$ system except for the chemical grafted DOX beads being replaced by the same amount of free DOX beads, and the results are shown in Figure 6B. It was found that in the system of the DOX physically loaded micelles, when the amount of free DOX beads increased from equal to the β-CD-P[CL_{30}-*co*-(ACL-*g*-DOX)$_y$-SS-$MPEG_{49}$]$_{21}$ system of y = 5 to equal to that of y = 14, not all DOX beads could be completely encapsulated into the polymeric micelles, and part of DOX beads were still floating outside, which resulted in the diminution of both DLC and DLE of the micelles, compared to the system of the prodrug unimolecular micelles. As shown in Figure 6D, though the DLC value gradually rose as the amount of feed DOX beads increased, they were all lower than that of the corresponding prodrug unimolecular micelles. For the DLE values, due to the existence of free DOX beads, they were all less than 100%, inferior to those of corresponding prodrug unimolecular micelles. The cutaway views shown in Figure 6B revealed that in the DOX physically loaded micelles, DOX beads were only distributed on the surface of the micellar hydrophobic core and almost no DOX bead entered the core. While the cutaway views shown in Figure 6A showed that in the prodrug

https://doi.org/10.1021/acsomega.2c07371
ACS Omega 2023, 8, 4963−4971

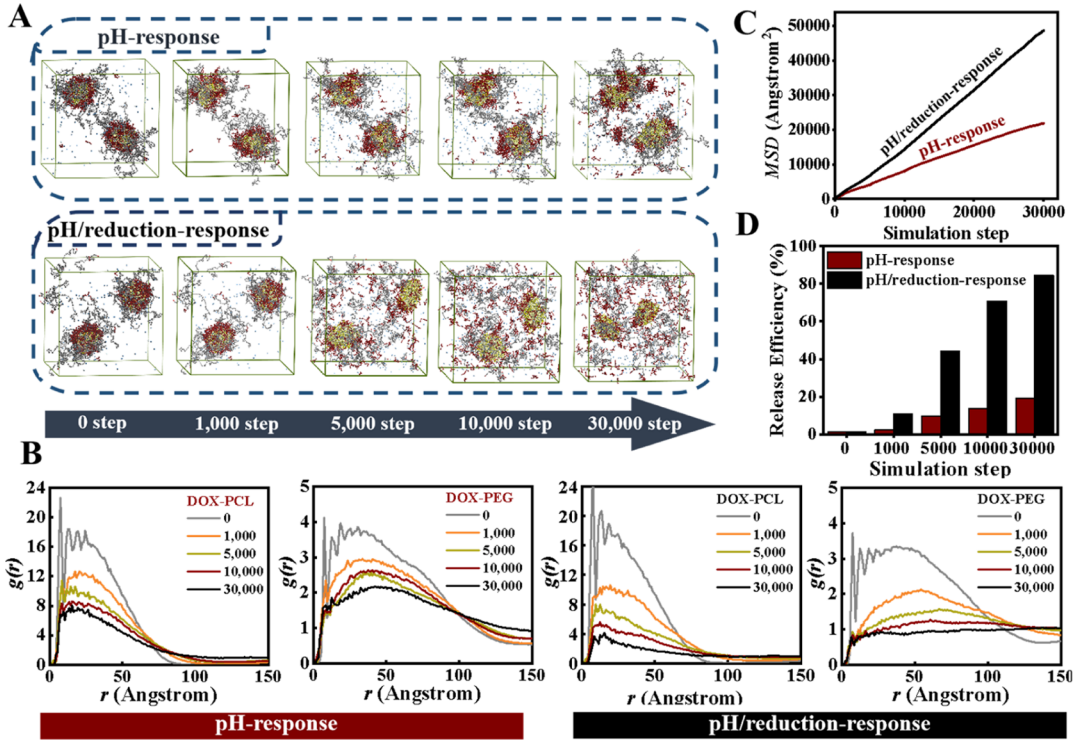

Figure 7. DPD simulations for the pH-responsive and dual pH/reduction-responsive DOX release process (A) and their corresponding RDF curves (B), MSD curves (C), and DOX release efficiency diagram (D) calculated from simulation results.

micelles, except for most of the DOX beads distributed at the interface between the hydrophobic core and the hydrophilic shell, when the amount of DOX beads increased, more and more DOX beads appeared inside the hydrophobic core. It further confirmed that the superiority of the prodrug strategy on the drug loading capacity of the micelles.

On the other hand, by comparing the equilibrium aggregation morphologies of the prodrug micelles in Figure 6A and the DOX physically loaded micelles in Figure 6B, it was also found that the prodrug micelles could avoid drug leakage, while in the DOX physically loaded micelles, drug release in advance or drug leakage during the delivery of the micelles in the aqueous solution could not be completely avoided.

3.6. Drug Release Performance of Prodrug Unimolecular Micelles. The ability of drug-controlled release in targeted tissues was an important criterion to evaluate whether the drug release behavior of micelles was enough for their desired purpose. In this study, the DOX release behavior of the prodrug unimolecular micelles β-CD-P[CL-*co*-(ACL-*g*-DOX)-SS-MPEG$_{]21}$ was achieved by dual responding to a slightly acidic condition and a high concentration of glutathione in the tumor microenvironment by the cleavage of β-carboxylic amide (NCD-DOX) bonds and the disulfide (−SS−) bonds. In our study, for pH-responsive and pH/reduction-responsive release, the pH value in the tumor environment was set at 5.0 In this condition, when pK_a = 6.9 was used, the protonation degree of ACL, NCD, and DOX was 98.8%, which could be calculated from the Hasselbach−Henderson equation.[43] Here, to simplify the simulation, it was assumed that all of the ACL, NCD, and DOX beads changed into ACLH, NCDH, and DOXH beads, which meant β-carboxylic amide was completely broken. To predict the dual responsive behavior and better understand the DOX release mechanism of the system, by employing a special bond-breaking script, DPD simulations for the pH-responsive and the dual pH/reduction-responsive DOX release process were performed, respectively, and results are shown in Figure 7.

As shown in Figure 7A, in the slightly acidic condition, the pH-sensitive β-carboxylic amide (NCD-DOX) bonds would break, leading to the release of DOX. First, the DOX beads present a tendency to spread out of the micelles due to the cleavage of β-carboxylic amide bonds and the protonation of DOX3 (1000 steps). However, for the single pH-responsive system, since the prodrug unimolecular micelles themselves were thermodynamically stable and the hydrophilic MPEG protective shell was still existing after the cleavage of β-carboxylic amide bonds, the diffusion rate of the DOX beads was slow (5000 steps), and most of the DOX beads clumped distributed near the swelling micelles rather than completely free (30,000 step). Significantly faster escape behavior of DOX from the micelles was observed in the dual pH/reduction-responsive system, due to the cleavage of the disulfide bonds in the high concentration of glutathione, which resulted in the gradual abjunction of hydrophilic MPEG protective shell, (5000 steps), near disassembly of the micelles (10,000 step), the most release of DOX (30,000 steps). This result could be further supported by the RDF curves of DOX-PCL and PEG-PCL in Figure 7B.

The hydrophobic PCL beads were generally located in the original micellar center, which meant the RDF curves of DOX-PCL and PEG-PCL could be used to quantitatively investigate and analyze the DOX release behavior. As the simulation step increasing from 0 to 30,000 in both the single pH-responsive system and the dual pH/reduction-responsive system, it was found from the RDF curves of DOX-PCL that the DOX beads distributed in the PCL core gradually reduced, indicating the DOX beads began to spread outside the micelles in the slightly acidic condition. Compared to the single pH-responsive

https://doi.org/10.1021/acsomega.2c07371
ACS Omega 2023, 8, 4963−4971

system, the DOX diffusion rate in the dual pH/reduction-responsive system was accelerated due to the cleavage of the disulfide bonds in the reduction condition, which caused the separation of the MPEG. As shown by the RDF curves of PEG-PCL, in the single pH-responsive system, the peaks of the RDF curves all appeared at around 50 angstrom radius, which meant the PEG beads always distributed surrounding the PCL core when the simulation step increasing from 0 to 30,000, and the small divergence of the curves was mainly caused by the swelling of the micelles. While in the dual pH/reduction-responsive system, the separation of the MPEG from the micelles led to the dramatic change of peaks of the RDF curves when the simulation step increased, until the MPEG completely dissolved into the surrounding water, which resulted in the accelerated release of the DOX beads.

The mean square displacement (MSD) curves shown in Figure 7C could theoretically compare the DOX release rates between the single pH-responsive system and the dual pH/reduction-responsive system as their slopes were directly connected with the diffusion coefficient of the DOX. From the MSD curves, it was intuitively embodied that the locomotion activity of DOX beads in the dual pH/reduction-responsive system was quite higher than that in the single pH-responsive system, indicating its accelerated release of DOX beads. The release efficiency diagram shown in Figure 7D was obtained by evaluating the residual amount of DOX beads in micelles to the total DOX beads. It was also shown that the DOX release efficiency in the dual pH/reduction-responsive system was obviously higher than that in the single pH-responsive system. Therefore, it could be preliminarily concluded that the prodrug unimolecular micelles assembled by β-CD-P[CL_{30}-*co*-(ACL-*g*-DOX)$_8$-SS-MPEG$_{49}$]$_{21}$ would provide well dual pH/reduction-responsive DOX release performance, and was worthy of further experimental study.

4. CONCLUSIONS

DPD simulations on the self-assembly behavior and their formation conditions of the star-like polymeric prodrug unimolecular micelles formed by β-CD-P[CL-*co*-(ACL-*g*-DOX)-SS-MPEG]$_{21}$ showed that to form well monodispersed and superior DOX-loaded unimolecular micelles, the polymer concentration should be well controlled in a low volume fraction ($\leq$10.59%), and the detailed molecular structure of the polymer was suggested as β-CD-P[CL_{30}-*co*-(ACL-*g*-DOX)$_8$-SS-MPEG$_{49}$]$_{21}$. Compared the corresponding equilibrium aggregation morphologies, cutaway views, and DLE/DLC curves with those of the DOX physically loaded micelles, it was found that the prodrug unimolecular micelles displayed superior drug loading capacity and no drug leakage during the delivery. Simulations on the prodrug release process showed that the prodrug unimolecular micelles assembled by β-CD-P[CL_{30}-*co*-(ACL-*g*-DOX)$_8$-SS-MPEG$_{49}$]$_{21}$ could more effectively release DOX in the dual acidic and high concentration of glutathione condition, which was confirmed by the corresponding RDF curves, MSD curves, and DOX release efficiency diagram. This study verified the superiority of applying the prodrug strategy to unimolecular micelles on the mesoscopic scale and provide theoretical guidance on structure optimization and performance prediction of the unimolecular micelles with dual pH/reduction-responsive release.

AUTHOR INFORMATION

Corresponding Author

Chufen Yang − *School of Chemical Engineering and Light Industry, Guangdong University of Technology, Guangzhou 510006, PR China;* orcid.org/0000-0003-0793-1302; Phone: 86-020-39322231; Email: cfyang@gdut.edu.cn; Fax: 86-020-39322231

Authors

Zexiong Yang − *School of Chemical Engineering and Light Industry, Guangdong University of Technology, Guangzhou 510006, PR China*

Haiyan Mai − *Department of Pharmacy, Third Affiliated Hospital of Sun Yat-sen University, Guangzhou 510630, PR China*

Delin Wang − *School of Chemical Engineering and Light Industry, Guangdong University of Technology, Guangzhou 510006, PR China*

Teng He − *School of Chemical Engineering and Light Industry, Guangdong University of Technology, Guangzhou 510006, PR China*

Fang Chen − *School of Chemical Engineering and Light Industry, Guangdong University of Technology, Guangzhou 510006, PR China*

Complete contact information is available at: https://pubs.acs.org/10.1021/acsomega.2c07371

Author Contributions

Z.Y. and H.M. contributed equally to this work. Z.Y. and H.M.: conceptualization, methodology, and writing—original draft preparation. D.W.: software and data curation. T.H. and F.C.: visualization and investigation. C.Y.: conceptualization, methodology, writing—reviewing and editing, supervision, and validation.

Notes

The authors declare no competing financial interest.

ACKNOWLEDGMENTS

The authors gratefully acknowledge the financial support from the National Natural Science Foundation of China (no. 21676058) and the Natural Science Foundation of Guangdong Province (no. 2016A030313694).

REFERENCES

(1) Kalyane, D.; Raval, N.; Maheshwari, R.; Tambe, V.; Kalia, K.; Tekade, R. K. Employment of enhanced permeability and retention effect (EPR): Nanoparticle-based precision tools for targeting of therapeutic and diagnostic agent in cancer. *Mater. Sci. Eng., C* **2019**, *98*, 1252−1276.

(2) Iyer, A. K.; Khaled, G.; Fang, J.; Maeda, H. Exploiting the enhanced permeability and retention effect for tumor targeting. *Drug Discovery Today* **2006**, *11*, 81−818.

(3) Cabral, H.; Miyata, K.; Osada, K.; Kataoka, K. Block Copolymer Micelles in Nanomedicine Applications. *Chem. Rev.* **2018**, *118*, 6844−6892.

(4) Lu, Q.; Yi, M.; Zhang, M.; Shi, Z.; Zhang, S. Folate-Conjugated Cell Membrane Mimetic Polymer Micelles for Tumor-Cell-Targeted Delivery of Doxorubicin. *Langmuir* **2019**, *35*, 504−512.

(5) Lei, B.; Sun, M.; Chen, M.; Xu, S.; Liu, H. pH and Temperature Double-Switch Hybrid Micelles for Controllable Drug Release. *Langmuir* **2021**, *37*, 14628−14637.

(6) Lu, Y.; Yue, Z.; Xie, J.; Wang, W.; Zhu, H.; Zhang, E.; Cao, Z. Micelles with ultralow critical micelle concentration as carriers for drug delivery. *Nat. Biomed. Eng.* **2018**, *2*, 318−325.

https://doi.org/10.1021/acsomega.2c07371
ACS Omega 2023, 8, 4963−4971

(7) Lu, Y.; Zhang, E.; Yang, J.; Cao, Z. Strategies to improve micelle stability for drug delivery. *Nano Res.* **2018**, *11*, 4985−4998.
(8) Liu, X.; Fan, X.; Jiang, L.; Loh, X. J.; Wu, Y.-L.; Li, Z. Biodegradable polyester unimolecular systems as emerging materials for therapeutic applications. *J. Mater. Chem. B* **2018**, *6*, 5488−5498.
(9) Chen, W.; Liu, P. Pegylated dendritic polyurethane as unimolecular micelles for tumor chemotherapy: Effect of molecular architecture. *Int. J. Pharm.* **2022**, *616*, 121533.
(10) Tambe, P.; Kumar, P.; Paknikar, K. M.; Gajbhiye, V. Smart triblock dendritic unimolecular micelles as pioneering nanomaterials: Advancement pertaining to architecture and biomedical applications. *J. Controlled Release* **2019**, *299*, 64−89.
(11) Xue, Y. T.; Sun, J.; Xiong, S.; Chai, H. N.; Xin, X.; Xu, G. Y.; Liu, T. Effect of block sequence of hyperbranched block copolymers on the aggregation behavior, drug solubilization and release property. *J. Mol. Liq.* **2019**, *278*, 320−328.
(12) Jin, X.; Sun, P.; Tong, G. S.; Zhu, X. Y. Star polymer-based unimolecular micelles and their application in bio-imaging and diagnosis. *Biomaterials* **2018**, *178*, 738−750.
(13) Zhao, X. B.; Si, J. X.; Huang, D. S.; Li, K.; Xin, Y.; Sui, M. H. Application of star poly(ethylene glycol) derivatives in drug delivery and controlled release. *J. Controlled Release* **2020**, *323*, 565−577.
(14) Ren, J. M.; McKenzie, T. G.; Fu, Q.; Wong, E. H. H.; Xu, J.; An, Z.; Shanmugam, S.; Davis, T. P.; Boyer, C.; Qiao, G. G. Star Polymers. *Chem. Rev.* **2016**, *116*, 6743−6836.
(15) Lu, Y.; Zhang, E.; Yang, J.; Cao, Z. Strategies to improve micelle stability for drug delivery. *Nano Res.* **2018**, *11*, 4985−4998.
(16) Gao, Y.-E.; Bai, S.; Ma, X.; Zhang, X.; Hou, M.; Shi, X.; Huang, X.; Chen, J.; Wen, F.; Xue, P.; Kang, Y.; Xu, Z. Codelivery of doxorubicin and camptothecin by dual-responsive unimolecular micelle-based β-cyclodextrin for enhanced chemotherapy. *Colloids Surf., B* **2019**, *183*, 110428.
(17) Lepeltier, E.; Rijo, P.; Rizzolio, F.; Popovtzer, R.; Petrikaite, V.; Assaraf, Y. G.; Passirani, C. Nanomedicine to target multidrug resistant tumors. *Drug Resistance Updates* **2020**, *52*, 100704.
(18) Ma, B. X.; Zhuang, W. H.; Wang, Y. A.; Luo, R. F.; Wang, Y. B. pH-sensitive doxorubicin-conjugated prodrug micelles with charge-conversion for cancer therapy. *Acta Biomater.* **2018**, *70*, 186−196.
(19) Zhou, M.; Wen, L.; Wang, C.; Lei, Q.; Li, Y.; Yi, X. Recent Advances in Stimuli-Sensitive Amphiphilic Polymer-Paclitaxel Prodrugs. *Front. Bioeng. Biotechnol.* **2022**, *10*, 875034.
(20) Dong, C.; Zhou, Q.; Xiang, J.; Liu, F.; Zhou, Z.; Shen, Y. Self-assembly of oxidation-responsive polyethylene glycol-paclitaxel prodrug for cancer chemotherapy. *J. Controlled Release* **2020**, *321*, 529−539.
(21) Li, Y.; Yang, M.; Zhao, Y.; Li, L.; Xu, W. Preparation and in vitro evaluation of amphiphilic paclitaxel small molecule prodrugs and enhancement of oral absorption. *Eur. J. Med. Chem.* **2021**, *215*, 113276.
(22) Li, M.; Zhao, Y.; Sun, J.; Chen, H.; Liu, Z.; Lin, K.; Ma, P.; Zhang, W.; Zhen, Y.; Zhang, S.; Zhang, S. pH/reduction dual-responsive hyaluronic acid-podophyllotoxin prodrug micelles for tumor targeted delivery. *Carbohydr. Polym.* **2022**, *288*, 119402.
(23) Gao, Y. E.; Bai, S.; Ma, X. Q.; Zhang, X. L.; Hou, M. L.; Shi, X. X.; Huang, X. H.; Chen, J. C.; Wen, F. Q.; Xue, P.; Kang, Y. J.; Xu, Z. G. Codelivery of doxorubicin and camptothecin by dual-responsive unimolecular micelle-based β-cyclodextrin for enhanced chemotherapy. *Colloids Surf., B* **2019**, *183*, 110428.
(24) Deng, H. Z.; Liu, J. J.; Zhao, X. F.; Zhang, Y. M.; Liu, J. F.; Xu, S. X.; Deng, L. D.; Dong, A. J.; Zhang, J. H. PEG-b-PCL Copolymer Micelles with the Ability of pH-Controlled Negative-to-Positive Charge Reversal for Intracellular Delivery of Doxorubicin. *Biomacromolecules* **2014**, *15*, 4281−4292.
(25) Guo, H.; Liu, F. Z.; Liu, E. Q.; Wei, S. S.; Sun, W. B.; Liu, B. Q.; Sun, G. Y.; Lu, L. H. Dual-responsive nano-prodrug micelles for MRI-guided tumor PDT and immune synergistic therapy. *J. Mater. Chem. B* **2022**, *10*, 4261−4273.
(26) Wang, Y.; Li, Q. Y.; Liu, X. B.; Zhang, C. Y.; Wu, Z. M.; Guo, X. D. Mesoscale Simulations and Experimental Studies of pH-Sensitive Micelles for Controlled Drug Delivery. *ACS Appl. Mater. Interfaces* **2015**, *7*, 25592−25600.
(27) Wu, W. S.; Yi, P.; Zhang, J.; Cheng, Y. C.; Li, Z. W.; Hao, X. Y.; Chen, Q. 4/6-Herto-arm and 4/6-mikto-arm star-shaped block polymeric drug-loaded micelles and their pH-responsive controlled release properties: a dissipative particle dynamics simulation. *Phys. Chem. Chem. Phys.* **2019**, *21*, 15222−15232.
(28) Zeng, S. J.; Quan, X. B.; Zhu, H. L.; Sun, D. L.; Miao, Z. H.; Zhang, L. Z.; Zhou, J. Computer Simulations on a pH-Responsive Anticancer Drug Delivery System Using Zwitterion-Grafted Polyamidoamine Dendrimer Unimolecular Micelles. *Langmuir* **2021**, *37*, 1225−1234.
(29) Zhang, X. F.; Lin, W. J.; Wen, L. Y.; Yao, N.; Nie, S. Y.; Zhang, L. J. Systematic design and application of unimolecular star-like block copolymer micelles: a coarse-grained simulation study. *Phys. Chem. Chem. Phys.* **2016**, *18*, 26519−26529.
(30) Yang, C. F.; Yin, L.; Yuan, C.; Liu, W. Y.; Guo, J. W.; Shuttleworth, P. S.; Yue, H. B.; Lin, W. J. DPD simulations and experimental study on reduction-sensitive polymeric micelles self-assembled from PCL-SS-PPEGMA for doxorubicin controlled release. *Colloids Surf., B* **2021**, *204*, 111797.
(31) Yang, Z. X.; Zhao, H. Q.; Wang, D. L.; Yin, L.; Cai, K. X.; Lin, Z. H.; Chen, T.; Yang, C. F. DPD simulations on mixed polymeric DOX-loaded micelles assembled from PCL-SS-PPEGMA/PDEA-PPEGMA and their dual pH/reduction-responsive release. *Phys. Chem. Chem. Phys.* **2021**, *23*, 19011−19021.
(32) Hao, J.; Wang, J.; Pan, H.; Sang, Y.; Wang, D.; Wang, Z.; Ai, J.; Lin, B.; Chen, L. pH-redox responsive polymer-doxorubicin prodrug micelles studied by molecular dynamics, dissipative particle dynamics simulations and experiments. *J. Drug Delivery Sci. Technol.* **2022**, *69*, 103136.
(33) Feng, Y. H.; Zhang, X. P.; Zhao, Z. Q.; Guo, X. D. Dissipative Particle Dynamics Aided Design of Drug Delivery Systems: A Review. *Mol. Pharmaceutics* **2020**, *17*, 1778−1799.
(34) Santo, K. P.; Neimark, A. V. Dissipative particle dynamics simulations in colloid and Interface science: a review. *Adv. Colloid Interface Sci.* **2021**, *298*, 102545.
(35) Groot, R. D.; Rabone, K. L. Mesoscopic Simulation of Cell Membrane Damage, Morphology Change and Rupture by Nonionic Surfactants. *Biophys. J.* **2001**, *81*, 725−736.
(36) Hoogerbrugge, P. J.; Koelman, J. M. V. A. Simulating Microscopic Hydrodynamic Phenomena with Dissipative Particle Dynamics. *Europhys. Lett.* **1992**, *19*, 155−160.
(37) Li, W.; Chu, W.; Jian, Z. Dissipative Particle Dynamics Simulations on the pH-responsive Gating of Block Copolymer Brush Modified Nanopores. *Chem. J. Chin. Univ.* **2018**, *39*, 85−94.
(38) Zhu, G.; Yin, G.; Ding, J.; Tang, Q.; Shang, J.; Lin, X. Sodium Benzenesulfonate-Assisted Preparation of Lignosulfonate-Based Spherical Micelles: Insights from Mesoscopic Simulations. *ACS Sustainable Chem. Eng.* **2022**, *10*, 2262−2270.
(39) Wang, Y.; Zhu, D. D.; Zhou, J.; Wang, Q. L.; Zhang, C. Y.; Liu, Y. J.; Wu, Z. M.; Guo, X. D. Mesoscopic simulation studies on the formation mechanism of drug loaded polymeric micelles. *Colloids Surf., B* **2015**, *136*, 536−544.
(40) Hao, L.; Lin, L.; Zhou, J. pH-Responsive Zwitterionic Copolymer DHA−PBLG−PCB for Targeted Drug Delivery: A Computer Simulation Study. *Langmuir* **2019**, *35*, 1944−1953.
(41) Yang, C.; Yin, L.; Yuan, C.; Liu, W.; Guo, J.; Shuttleworth, P. S.; Yue, H.; Lin, W. DPD simulations and experimental study on reduction-sensitive polymeric micelles self-assembled from PCL-SS-PPEGMA for doxorubicin controlled release. *Colloids Surf., B* **2021**, *204*, 111797.
(42) Prhashanna, A.; Tan, W. K.; Khan, S. A.; Chen, S. B. Co-micellization behavior of triblock copolymers in the presence of hydrophobic drug molecules: A simulation study. *Colloids Surf., B* **2016**, *148*, 299−307.
(43) Wang, W. J.; Anderson, N. A.; Travesset, A.; Vaknin, D. Regulation of the Electric Charge in Phosphatidic Acid Domains. *J. Phys. Chem. B* **2012**, *116*, 7213−7220.

https://doi.org/10.1021/acsomega.2c07371
ACS Omega 2023, 8, 4963−4971